Microsecond Response in Organic Electrochemical Transistors: Exceeding the Ionic Speed Limit

*Jacob T. Friedlein, Mary J. Donahue, Sean E. Shaheen, George G. Malliaras, and Robert R. McLeod**

Organic electrochemical transistors (OECTs) are thin-film transistors that use an electrolyte as the dielectric material between the gate and channel. High-capacitance electrolyte/organic–semiconductor interfaces endow OECTs with extrinsic transconductances exceeding 400 S m^{-1}—larger than that demonstrated for a wide range of other transistor technologies.[1] OECTs operate at low voltages and can be used in aqueous environments, making them ideal for biosensing applications.[2–5] For instance, OECTs can be used for in vivo electrocorticographic (ECoG) arrays to detect epileptic activity[6] or in vitro to detect the activity of cardiac cells.[7] OECTs have also been used for long-term electrocardiogram recordings,[8,9] measuring metabolite concentration,[10–14] and monitoring barrier–cell properties.[15–19] Several reports also demonstrate OECT implementations of digital logic[20–23] and neuromorphic circuits.[24–26] The transient behavior of OECTs is critical in all of the applications mentioned above. For example, 10–100 kHz operation is necessary for high-accuracy resolution of neuron action potentials. In neuromorphic applications, the response speed following a gate pulse determines learning times, and in digital logic circuits transistor bandwidth is an important performance specification. Unfortunately, OECTs are slow devices, with time constants typically on the order of 1–100 ms[8,27–29] and sometimes larger than 1 s.[30–34] These slow speeds are an inherent consequence of the switching mechanism in OECTs, which relies on the injection of ions into the transistor channel. The time constant for ion injection determines the limiting speed for the OECT, independent of hole drift times along the channel. This ionic speed is a severe limitation for device performance because strategies to increase the ionic speed degrade other performance parameters. For instance, decreasing channel thickness increases switching speed but causes a proportional decrease in transconductance.[1,35] Similarly, decreasing the concentration of secondary polar dopants increases device speed but decreases channel conductance and transconductance.[36] Also, removing the cross-linker 3-glycidoxypropyltrimethoxysilane increases device speed but allows delamination during device operation.[37,38] Here, we demonstrate that the slow ionic speed of OECTs need not limit their performance. We find that the OECT response can be made 30 times faster than its ionic speed when the drain bias is tuned to the step-response voltage, V_{step}. Furthermore, we provide a model that accounts for this high-speed behavior and can be used to understand the transient response of OECTs in a variety of applications.

OECT behavior is described in the literature and is briefly reviewed here.[39–42] **Figure 1**a shows the structure of a typical OECT. The transistor's output current flows through the channel composed of the organic semiconductor poly(3,4-ethylenedioxythiophene) doped with poly(styrene sulfonate) (PEDOT:PSS). The PSS anions are somewhat analogous to acceptor ions in inorganic semiconductors. They provide a counter charge for holes on the PEDOT chain and make the OECT channel conductive. A positive input voltage at the gate electrode modulates the channel current by pushing cations from the electrolyte into the PEDOT:PSS matrix. The cations form ionic bonds with the PSS, compensating the counter charge for holes and thus decreasing the hole concentration in the PEDOT. Removing holes from the PEDOT makes the channel less conductive and decreases the OECT's output current. Alternatively, a negative gate voltage pushes anions into the channel, increasing the hole concentration and thus increasing the OECT's output current. To date, every reported OECT has operated no faster than the time required to charge the transistor channel with the ionic species. This ionic time constant is analogous to the RC time constant of a simple resistor–capacitor (RC) circuit, and because it is determined by ion transport into the bulk of an organic film, it is typically quite slow—even reportedly fast devices have time constants of ≈1 ms.[28]

Although ion transport is an essential part of OECT operation and usually determines the response speed, we show that it is possible to overcome this limitation. **Figure 2** shows the source current response to a gate voltage step from 20 to 0 mV with a constant drain voltage. We tested the OECT with the drain voltage fixed at −30 mV (Figure 2a,d), −80 mV (Figure 2b,e), and −130 mV (Figure 2c,f). At −30 and −130 mV the source current exponentially relaxes to steady-state in ≈600 µs, but in Figure 2b the change in source current settles to within 10% of its final value in only 20 µs. We can compare this 20 µs response to the ionic speed by measuring the gate current, which is equal to the ionic charging current of the OECT. Figure 2e shows

J. T. Friedlein, Prof. S. E. Shaheen, Prof. R. R. McLeod
Department of Electrical, Computer and Energy Engineering
University of Colorado
Campus box 425, Boulder, CO 80309-0425, USA
E-mail: robert.mcleod@colorado.edu
Dr. M. J. Donahue, Prof. G. G. Malliaras
Department of Bioelectronics
Ecole Nationale Supérieure des Mines
CMP-EMSE, MOC
13541 Gardanne, France
Prof. S. E. Shaheen
Department of Physics
University of Colorado
Campus box 390, Boulder, CO 80309-0390, USA

DOI: 10.1002/adma.201602684

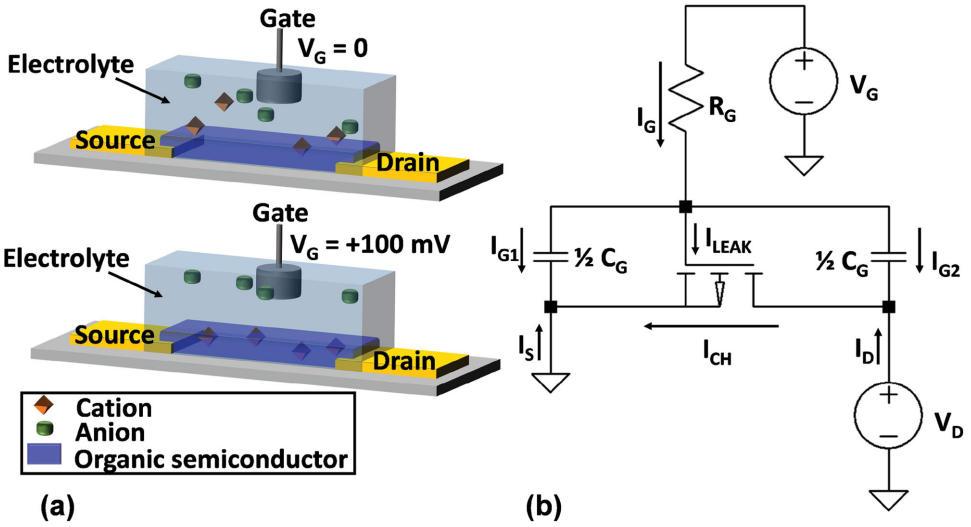

Figure 1. a) Structure and operation of a typical OECT with a PEDOT:PSS channel. Top: OECT channel in the high-conductivity state with a gate voltage of 0 V. Bottom: The gate voltage of +100 mV pushes cations into the OECT channel. These cations de-dope the organic semiconductor, lowering its conductivity. b) Circuit diagram of the discrete model showing the gate current branches and the distinct source (I_S), drain (I_D), and channel (I_{CH}) currents.

the gate current corresponding to the source current shown in Figure 2b. The gate current is an exponential function with a time constant of 300 µs and requires more than 690 µs to settle to less than 10% of its peak value. Therefore, the source current response exceeds the speed of the ionic circuit by more than a factor of 30.

This observation of source current response speed exceeding the ionic speed has not been previously reported. However, we can explain this faster-than-ionic response by building on previous descriptions of OECT behavior.[13,41–44] Bernards and Malliaras modeled OECT behavior with a standard long-channel field-effect transistor (FET) and a series RC circuit between the gate and channel.[42] The FET describes the steady-state behavior of the OECT, and the RC circuit describes the ionic coupling through the electrolyte between the gate and the channel. This RC series can be understood as an approximation for equivalent circuits typically used to describe ion transport.[45–48] The RC time constant of this ionic circuit determines the limiting speed of the electronic OECT response, regardless of electronic transit times along the channel.[42] Despite finding this, the Bernards model does not provide a closed-form expression for OECT transient behavior because it fails to account for spatially varying hole currents in the channel before steady-state is reached. Forchheimer and co-workers provide a model without this shortcoming by describing the transient behavior of electrolyte-gated FETs with the Ward–Dutton partition scheme.[43] Forchheimer and co-workers' model highlights the fact that the source and drain currents are not necessarily equal because the transient gate current contributes differently at the source and drain terminals. Our discrete model follows the work of Bernards and Forchheimer, describing the ionic circuit with a series RC, and allowing unequal source and drain currents in the transient regime.

The discrete model is depicted in Figure 1b and consists of four discrete circuit elements—a resistor describing the ionic resistance between the gate electrode and the transistor channel,[42,49] two capacitors describing the accumulation of ionic charge in the transistor channel,[35,42] and an ideal p-channel FET describing the OECT's steady-state current–voltage relationships.[42] According to the discrete model, when the leakage current, I_{leak}, is negligible, the source current is given by Equation (1):

$$\begin{aligned} I_S &= -(I_{CH} + I_{G1}) \\ I_D &= I_{CH} - I_{G2} \end{aligned} \tag{1}$$

If the source and drain voltages are constant with respect to time and the OECT geometry is symmetric, exactly half of the gate current flows to the source terminal and half flows to the drain terminal. If the gate voltage is a square step, the channel current is $I_{CH}(t) = I_{CH}(0) + \Delta I_{CH}[1 - \exp(-t/\tau_{RC})]$, and the gate current is $I_G(t) = I_{G,max}\exp(-t/\tau_{RC})$ (see the Supporting Information). The ionic RC time constant, τ_{RC}, limits the response speed of the OECT; however, when $\Delta I_{CH} = 0.5\, I_{G,max}$, the source current will respond to a square voltage step with a square current step. Each row of Figure 2 corresponds to a different drain voltage, and, because increasing the drain voltage increases ΔI_{CH} but does not affect $I_{G,max}$, each row of Figure 2 also corresponds to a different $\Delta I_{CH}/I_{G,max}$ ratio. Figure 2c,f shows the monotonic regime; in this regime the source current has a small positive step followed by an exponential increase until steady state is reached. The monotonic regime occurs when V_D is large enough that $\Delta I_{CH} > 0.5\, I_{G,max}$, as shown in Figure 2f. Figure 2a,d describes the opposite behavior, the spike-and-recover regime. In this regime, the source current displays a large positive step followed by an exponential decrease until steady state is reached. As shown in Figure 2d, this regime occurs when V_D is small enough that $0.5\, I_{G,max} > \Delta I_{CH}$. At the boundary between the monotonic and the spike-and-recover regimes is the step-response voltage, V_{step}. When $V_D = V_{step}$,

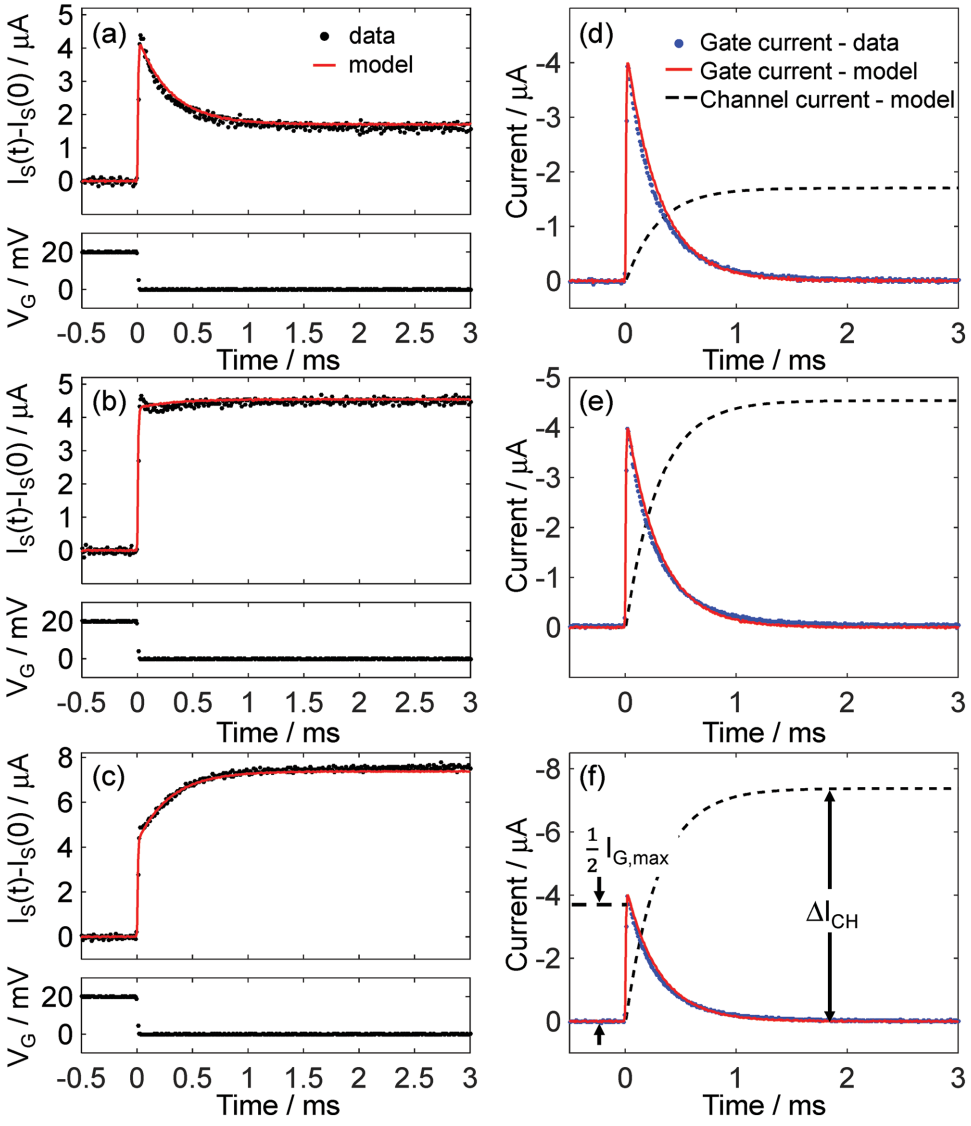

Figure 2. a–c) Change in the source current following a gate voltage step. d–f) Gate current and the change in channel current corresponding to the source currents shown in (a)–(c). The drain voltage is −30 mV for (a) and (d), −80 mV for (b) and (e), and −130 mV for (c) and (f). The gate voltage waveform is shown in the lower one-third of the panel in (a)–(c). In all panels, the data were averaged over 16 repeated waveforms. The resulting averages are plotted as dots and model fits are plotted as solid or dashed lines. The device had a channel width of W = 260 µm, a channel length of L = 100 µm, and a channel thickness of approximately h = 150 nm.

the source current responds with a step function. As shown in Figure 2e, this step response occurs when $0.5\, I_{G,max} = \Delta I_{CH}$. At the step-response voltage, the transient components of the gate and channel currents cancel each other at the source terminal, and the source current steps almost instantaneously from one steady-state value to another.

The shape of the source current varies greatly among Figure 2a–c, yet the data all come from the same device with the same intrinsic properties. This is made apparent by Figure 2d–f, which shows that the corresponding gate currents can each be fit with a single exponential and a time constant of 300 µs. This demonstrates that the source current responds faster at −80 mV than at −30 mV and −130 mV even though τ_{RC} is the same for all three cases. Being able to vary the transient operation regime could be useful in applications that require faster-than-ionic responses. For instance, a 20 µs step response is certainly fast enough to drive video displays,[50] and in neuromorphic devices, relaxation into the long-term-memory state would be much faster if the OECT were biased at V_{step}. However, restrictions on the step-response regime may limit its usefulness in other applications. For instance, V_{step} may not be large enough to drive a light-emitting diode and will lead to a less than unity current gain ($\Delta I_G/\Delta I_D$) at high frequencies (≳400 Hz). Also, logic circuits will have to be carefully designed to rely on the response speed at the positive end of the OECT channel (source current) rather than at the negative end of the channel (drain current).

The results in Figure 2 not only demonstrate a method of exceeding the ionic speed of an OECT, but also demonstrate the

robustness of our discrete model. This model uses four parameters to describe the OECT response to an arbitrary gate voltage. The four parameters are the ionic resistance, R_G; the ionic capacitance, C_G; a hole mobility, μ, describing the electronic mobility of the holes in the transistor channel; and a pinch-off voltage, V_P describing the voltage at which the OECT transitions from linear to saturation behavior.[35,41,42] In this Communication, all measurements are made in the linear regime, so V_P can be eliminated from the expressions for changes in the source, drain, and gate currents. The discrete model's fit to the source and gate currents is shown with solid red lines in Figure 2. Even though Figure 2 shows all three transient operating regimes, the data are all simultaneously fit by the discrete model with the same three fit parameters: $R_G = 2340 \pm 90\ \Omega$, $C_G = 127 \pm 6$ nF, and $\mu = 2.2 \pm 0.1\ cm^2\ V^{-1}\ s^{-1}$.

Not only does the discrete model predict faster-than-ionic OECT operation but also predicts the response to other gate voltage waveforms. **Figure 3** shows the source and drain currents as well as the discrete model fit in response to a 20 mV gate voltage step (Figure 3a), a 1 mV Lorentzian gate voltage spike (Figure 3b), and a series of 10 mV sine waves at different frequencies (Figure 3c). These input waveforms were chosen because of their relevance to several OECT sensing and logic applications. Square inputs have been used for enzymatic sensing,[10] detecting barrier cell integrity,[15,16,18] digital logic circuits,[21,22] and neuromorphic processing.[24,25] Lorentzian spikes mimic the shape of neuron action potentials that might be detected by ECoG arrays, and sine waves are used to characterize the frequency-domain behavior of OECTs for biosensing applications and analog circuit performance.[9,17,51]

Figure 3 shows that the discrete model simultaneously fits the responses to these different waveform shapes, amplitudes, and frequencies using only three free parameters. These model fits are shown in Figure 3 as solid lines, and the device parameters extracted from the fits are $R_G = 3090 \pm 50\ \Omega$, $C_G = 92 \pm 1$ nF, and $\mu = 3.19 \pm 0.05\ cm^2\ V^{-1}\ s^{-1}$—all of which are within the range of typical values reported in the literature.[35,52,53]

Figure 3 demonstrates that the utility of our discrete model reaches beyond the scope of applications that require faster-than-ionic responses. In particular, the discrete model highlights the difference between the source and drain currents in high-frequency measurements, such as those shown in Figure 3a,b. Figure 3b shows the source and drain responses to a Lorentzian-shaped gate voltage pulse. As predicted by the discrete model, the source current lags behind the gate excitation by less than 100 µs, but the drain current lags behind the excitation by ≈300 µs. Without the discrete model, this time delay could confound the interpretation of transient measurements. For instance, neuron action potentials generate voltage signals with shapes similar to the input voltage used for Figure 3b, and delay times between action potentials from different neurons indicate the presence or lack of neural connections.[54] Therefore, mapping neural connectivity with OECT-based arrays depends on a complete understanding of the time delays between input voltages and output currents.

Not only is the discrete model useful for interpreting high-frequency measurements, but it also can be used to estimate device parameters. The discrete model even describes a frequency-domain measurement of mobility that does not rely on

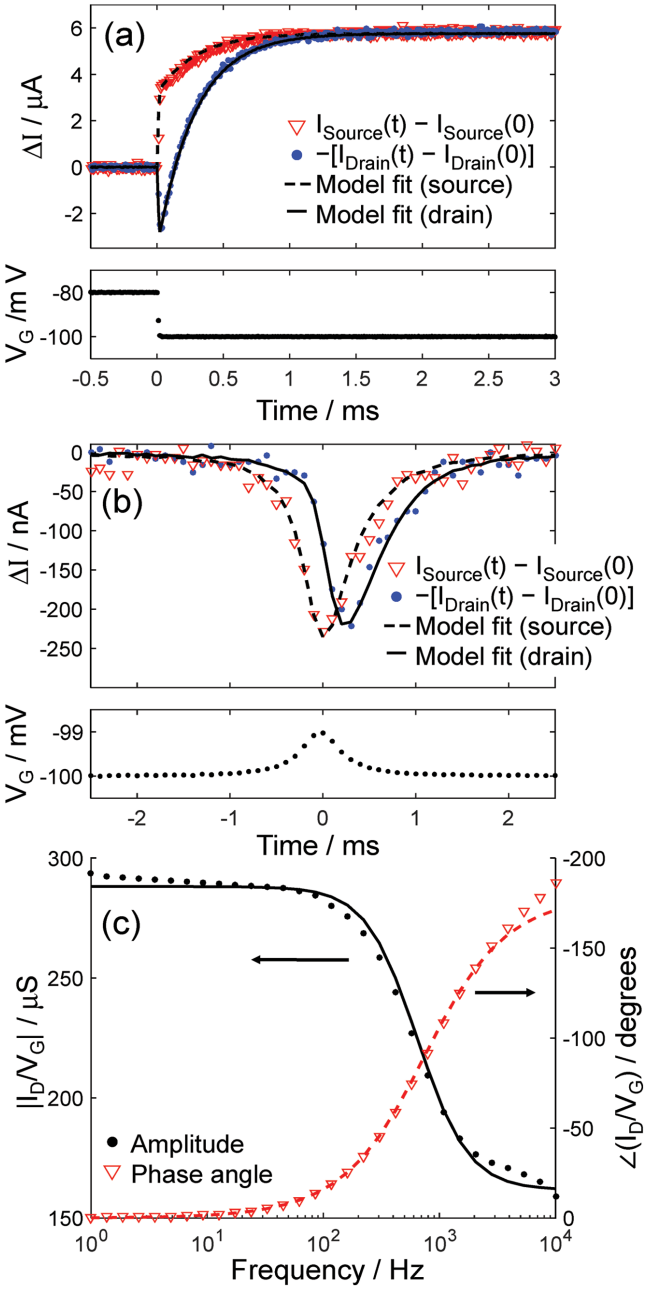

Figure 3. a) Change in source and drain currents, ΔI, responding to a square gate voltage step. b) ΔI for a Lorentzian voltage spike. c) Amplitude and phase of the transconductance as a function of the frequency of the sinusoidal gate voltage. In (a) and (b), the gate voltage waveform is on the lower one-third of the panel. In (a)–(c), the drain voltage is kept constant at $V_D = -100$ mV. In (a) and (b) the drain current is always negative, and the source current is always positive. We plotted the negative change in the drain current to facilitate comparison between the source and drain currents. In (a) and (b), the data were averaged over 19 and 24 waveform cycles, respectively. In (c), four frequency sweeps were performed. In (a)–(c) the resulting averages are plotted as dots, and the model fits are plotted as solid or dashed lines. The device geometry was $W = 255$ µm, $L = 100$ µm, and $h \approx 150$ nm.

estimates of any other parameters. As shown in the Supporting Information, the gate and drain current amplitudes are equal at the frequency given by Equation (2):

$$\omega_0 = 2\mu V_D/\left(\sqrt{3}L^2\right) \quad (2)$$

where ω_0 is radial frequency, μ is hole mobility, V_D is drain voltage, and L is channel length. We have shown that this measurement technique yields a mobility of 2.3 ± 0.4 $cm^2\ V^{-1}\ s^{-1}$ for the OECT used in Figure 2 and a mobility of 3.18 ± 0.6 $cm^2\ V^{-1}\ s^{-1}$ for the OECT used in Figure 3. These values agree with the mobilities from the time-domain measurements and are within the experimentally reported values for PEDOT:PSS-based OECTs.[35,53]

While proper design, operation, and interpretation of results are critical for OECT applications, the development of new materials is equally important. PEDOT:PSS is currently the champion material for OECTs, but because it contains the dopant PSS^-, it can only be used for depletion-mode OECTs.[20,42,51,55] This is a major drawback for both sensing and logic applications, and several materials for accumulation-mode OECTs have been developed.[55,56] We tested the generality of our model by fabricating an accumulation-mode OECT using an undoped polythiophene. We found that our model fits the time domain response of this accumulation-mode OECT and that the OECT is capable of a step response when biased at V_{step} (see Figure S6, Supporting Information).

The discrete model accurately describes transient behavior for a variety of input waveforms and biases, but it fails to take into account several non-idealities that affect OECTs. For example, our previous work showed that the ideal FET model is only valid over a limited voltage range because of the non-uniform mobility in organic semiconductors.[52] Several other researchers have demonstrated OECT behavior that departs from the long-channel FET model[7,39,51,57] and have reported non-uniform mobility in PEDOT:PSS.[53] Because the long-channel FET model is only valid for a limited range of voltages, the discrete model works best for small-signal excitations of less than 100 mV. This will not decrease the utility of the discrete model for biosensing because many biosensing applications involve measuring small excitations on the order of millivolts. For instance, action potentials only produce an ≈100 mV signal, which may be attenuated by tissue before reaching the OECT.[7,58,59] Another complication for OECTs is the presence of current drift even after many RC time constants. This effect is noticeable in our devices, but only after more than 10 RC time constants (≈3 ms) and with an amplitude of less than 500 nA (see Figure S3, Supporting Information), so it has a limited effect on transient measurements. This long-time-scale drift could be due to a number of processes, such as conformational changes in the polymer matrix,[60] concentration-dependent ionic mobility,[61,62] or gradual redox processes due to dissolved hydrogen and oxygen in the electrolyte.[63–65] These processes might also cause asymmetric turn-on and turn-off speeds, especially for large voltage steps. Designing OECTs with thick channels ($h \approx 2\sqrt{D\tau_{RC}} \approx 1.8\,\mu m$, where D is the ionic diffusion coefficient) will add further complications because diffusion of the ions through the channel will be slower than polarization of the electrolyte and ion drift in the electrolyte.[66,67] Although the discrete model overlooks these complexities inherent in OECTs, it is accurate for transient measurements in the small-signal regime, and one can adapt the model to describe non-idealities. For instance, non-uniform hole mobility can be accounted for by adding a disorder parameter to the steady-state equations used in the long-channel FET model,[52] and the non-ideal transient behavior can be described by allowing the capacitances to be dependent on voltage.[43] The discrete model strikes a balance between simplicity and accuracy and can be made more accurate at the expense of increased complexity.

Our results show that even in its most simple form, the discrete model is accurate down to time scales of ≈10 µs, but we were unable to test its accuracy on smaller time scales because of the ≈10 µs settling time of our source-meter unit. Although higher bandwidth measurements might not be necessary in biosensing applications, they could advance our understanding of OECTs by identifying the processes that limit the maximum response speed at the step-response voltage.

In conclusion, we showed that when biased at V_{step}, OECTs respond more than 30 times faster than the speed of the ionic charging circuit. We demonstrated that these high-speed transistors responded to a step input voltage with a step output current, settling to within 10% of the steady-state current in only 20 µs. We also developed a simple discrete model that described this high-speed behavior and can be used to predict the current response following an arbitrary gate input. This simple model uses only three fit parameters and can be implemented in circuit simulation software or described with closed-form expressions, so it will be useful for a wide range of OECT applications. Although our model overlooks some of the complexities inherent in OECTs, it will be accurate for biosensing applications, such as ECoG measurements, where input voltages do not vary by more than 100 mV. Overall, our work reveals that the shape and speed of the OECT transient response depend strongly on the applied drain bias, and that at the right bias, the current response can reach its steady-state value almost instantaneously.

Experimental Section

OECT Fabrication: OECTs were fabricated using a previously reported technique.[68] Gold electrodes were evaporated onto glass substrates and patterned via photolithographic liftoff. After this, an ≈2 µm layer of parylene-C was evaporated onto the substrate. Then an anti-adhesion layer (1% Micro-90 in water) was spun on before evaporating on a second layer of parylene-C. The parylene layers were patterned via reactive ion etching with a photolithographically patterned mask of AZ-9260. After etching, a PEDOT:PSS solution (95 wt% Clevios PH-1000, 4 wt% ethylene glycol, 0.9 wt% 3-glycidoxypropyltrimethoxysilane, 0.1 wt% dodecylbenzenesulfonic acid) was spun onto the parylene layer at 3000 rpm for 30 s and baked at 95 °C for 75 s. Next, the sacrificial layer of parylene-C was peeled off of the substrate, leaving PEDOT:PSS films in the transistor channels and a barrier layer of parylene-C covering the gold electrodes. Finally, the sample was baked on a hotplate at 140 °C for 70 min and subsequently immersed in water for 4 h.

Characterization: OECTs were characterized using a dual-channel source-meter unit (Agilent B2962a) with custom-written control code in Python. All measurements were made using an Ag/AgCl pellet (2 mm diameter × 2 mm height) as the gate electrode. The electrolyte was a solution of 100×10^{-3} M NaCl in water and was contained in a PDMS well on top of the OECTs. The time step between measurements was 10 µs for Figures 2 and 3a and 100 µs for Figure 3b. Because the source and drain currents could not be measured simultaneously, they were measured in consecutive experiments ≈1 min apart. The drain current

was measured with a negative drain voltage applied to the drain terminal and the source terminal at 0 V. The source current was measured by floating the source-meter channels up to the drain voltage. For example, the source current shown in Figure 2c was measured with +130 mV applied at the source terminal and 0 V applied at the drain terminal. The gate voltage for this measurement was stepped from +130 to +150 mV at time $t = 0$.

Characterization of the accumulation-mode OECT was the same as that of the PEDOT:PSS devices except that we used two digital multimeters (NI-PXI-4071) to measure the gate and drain currents while biasing the gate and drain with a multi-channel data acquisition card (NI-PXI 6289). A custom-written Labview control software was used for these measurements.

Estimation of Parameter Uncertainty: The fit parameters were estimated using custom code incorporating the nonlinear fit function lsqcurvefit from MATLAB R2015a. The fits were made between the discrete model and the frequency-domain data with upper and lower bounds on the mobility provided by the time-domain data. The measured gate voltage was used as the input for the discrete model calculations because the actual gate voltages are not perfect step functions or smooth Lorentzians. The ± uncertainties for the fit parameters are 95% confidence intervals extracted using the lsqcurvefit Jacobian and MATLAB's nlparci function. The uncertainties for the mobility measurements using Equation (2) were calculated by propagating the uncertainty in frequency (± half the step size between frequency samples).

Supporting Information

Supporting Information is available from the Wiley Online Library or from the author.

Acknowledgements

The authors acknowledge Prof. Iain McCulloch and Dan-Tiberiu Sbircea for the synthesis and donation of the material for the accumulation-mode OECT. The authors also acknowledge Dr. Jonathan Rivnay for lending his expertise in discussions leading to this Communication. This Communication is based upon work supported by the National Science Foundation Graduate Research Fellowship under Grant No. DGE 1144083, and NSF grant NSF EPMD 1509909. J.T.F. acknowledges support from the Graduate Assistantships in Areas of National Need Award No. P200A120063 and the NSF GRFP Award No. DGE 1144083. S.E.S. acknowledges support from the National Science Foundation grant DMR-1006930. R.R.M. acknowledges support from the National Science Foundation grant CAREER (ECCS 0847390). R.R.M. and S.E.S. acknowledge support from the National Science Foundation grant ECCS 1509909.

Received: May 20, 2016
Revised: June 21, 2016
Published online: July 26, 2016

[1] D. Khodagholy, J. Rivnay, M. Sessolo, M. Gurfinkel, P. Leleux, L. H. Jimison, E. Stavrinidou, T. Hervé, S. Sanaur, R. M. Owens, G. G. Malliaras, *Nat. Commun.* **2013**, *4*, 2133.
[2] P. Lin, F. Yan, *Adv. Mater.* **2012**, *24*, 34.
[3] G. Tarabella, F. M. Mohammadi, N. Coppedè, F. Barbero, S. Iannotta, C. Santato, F. Cicoira, *Chem. Sci.* **2013**, *4*, 1395.
[4] X. Strakosas, M. Bongo, R. M. Owens, *J. Appl. Polym. Sci.* **2015**, *132*, 41735.
[5] C. Liao, M. Zhang, M. Y. Yao, T. Hua, L. Li, F. Yan, *Adv. Mater.* **2015**, *27*, 7493.
[6] D. Khodagholy, T. Doublet, P. Quilichini, M. Gurfinkel, P. Leleux, A. Ghestem, E. Ismailova, T. Hervé, S. Sanaur, C. Bernard, G. G. Malliaras, *Nat. Commun.* **2013**, *4*, 1575.
[7] C. Yao, Q. Li, J. Guo, F. Yan, I. M. Hsing, *Adv. Healthcare Mater.* **2015**, *4*, 528.
[8] A. Campana, T. Cramer, D. T. Simon, M. Berggren, F. Biscarini, *Adv. Mater.* **2014**, *26*, 3874.
[9] P. Leleux, J. Rivnay, T. Lonjaret, J.-M. Badier, C. Bénar, T. Hervé, P. Chauvel, G. G. Malliaras, *Adv. Healthcare Mater.* **2015**, *4*, 142.
[10] S. Y. Yang, F. Cicoira, R. Byrne, F. Benito-Lopez, D. Diamond, R. M. Owens, G. G. Malliaras, *Chem. Commun.* **2010**, *46*, 7972.
[11] D. Khodagholy, V. F. Curto, K. J. Fraser, M. Gurfinkel, R. Byrne, D. Diamond, G. G. Malliaras, F. Benito-Lopez, R. M. Owens, *J. Mater. Chem.* **2012**, *22*, 4440.
[12] P. N. Bartlett, *Analyst* **1998**, *123*, 387.
[13] D. A. Bernards, D. J. Macaya, M. Nikolou, J. A. DeFranco, S. Takamatsu, G. G. Malliaras, *J. Mater. Chem.* **2008**, *18*, 116.
[14] L. Kergoat, B. Piro, D. T. Simon, M. C. Pham, V. Noel, M. Berggren, *Adv. Mater.* **2014**, *26*, 5658.
[15] L. H. Jimison, S. A. Tria, D. Khodagholy, M. Gurfinkel, E. Lanzarini, A. Hama, G. G. Malliaras, R. M. Owens, *Adv. Mater.* **2012**, *24*, 5919.
[16] M. Ramuz, K. Margita, A. Hama, P. Leleux, J. Rivnay, I. Bazin, R. M. Owens, *ChemPhysChem* **2015**, *16*, 1210.
[17] M. Ramuz, A. Hama, J. Rivnay, P. Leleux, R. M. Owens, *J. Mater. Chem. B* **2015**, *3*, 5971.
[18] M. Ramuz, A. Hama, M. Huerta, J. Rivnay, P. Leleux, R. M. Owens, *Adv. Mater.* **2014**, *26*, 7083.
[19] C. Yao, C. Xie, P. Lin, F. Yan, P. Huang, I.-M. Hsing, *Adv. Mater.* **2013**, *25*, 6575.
[20] D. Nilsson, N. Robinson, M. Berggren, R. Forchheimer, *Adv. Mater.* **2005**, *17*, 353.
[21] R. Mannerbro, M. Ranlöf, N. Robinson, R. Forchheimer, *Synth. Met.* **2008**, *158*, 556.
[22] P. C. Hütter, T. Rothlander, G. Scheipl, B. Stadlober, *IEEE Trans. Electron Devices* **2015**, *62*, 4231.
[23] D. Nilsson, *Ph.D. Thesis*, Linkoping University, Linkoping, Sweden, **2005**.
[24] P. Gkoupidenis, N. Schaefer, B. Garlan, G. G. Malliaras, *Adv. Mater.* **2015**, *27*, 7176.
[25] P. Gkoupidenis, N. Schaefer, X. Strakosas, J. A. Fairfield, G. G. Malliaras, *Appl. Phys. Lett.* **2015**, *107*, 263302.
[26] V. A. Demin, V. V. Erokhin, A. V. Emelyanov, S. Battistoni, G. Baldi, S. Iannotta, P. K. Kashkarov, M. V. Kovalchuk, *Org. Electron.* **2015**, *25*, 16.
[27] P.-O. Svensson, D. Nilsson, R. Forchheimer, M. Berggren, *Appl. Phys. Lett.* **2008**, *93*, 203301.
[28] P. A. Ersman, D. Nilsson, J. Kawahara, G. Gustafsson, M. Berggren, *Org. Electron.* **2013**, *14*, 1276.
[29] T. Rothlander, P. C. Hutter, E. Renner, H. Gold, A. Haase, B. Stadlober, *IEEE Trans. Electron Devices* **2014**, *61*, 1515.
[30] H. Toss, C. Suspène, B. Piro, A. Yassar, X. Crispin, L. Kergoat, M.-C. Pham, M. Berggren, *Org. Electron.* **2014**, *15*, 2420.
[31] H. Tang, P. Kumar, S. Zhang, Z. Yi, G. De Crescenzo, C. Santato, F. Soavi, F. Cicoira, *ACS Appl. Mater. Interfaces* **2015**, *7*, 969.
[32] G. Tarabella, G. Nanda, M. Villani, N. Coppedè, R. Mosca, G. G. Malliaras, C. Santato, S. Iannotta, F. Cicoira, *Chem. Sci.* **2012**, *3*, 3432.
[33] J. T. Mabeck, J. A. DeFranco, D. A. Bernards, G. G. Malliaras, S. Hocd , C. J. Chase, S. Hocdé, C. J. Chase, *Appl. Phys. Lett.* **2005**, *87*, 13503.
[34] P. C. Hütter, T. Rothländer, A. Haase, G. Trimmel, B. Stadlober, *Appl. Phys. Lett.* **2013**, *103*, 15.
[35] J. Rivnay, P. Leleux, M. Ferro, M. Sessolo, A. Williamson, D. A. Koutsouras, D. Khodagholy, M. Ramuz, X. Strakosas,

R. M. Owens, C. Benar, J.-M. Badier, C. Bernard, G. G. Malliaras, *Sci. Adv.* **2015**, *1*, e1400251.
[36] J. Rivnay, S. Inal, B. A. Collins, M. Sessolo, E. Stavrinidou, X. Strakosas, C. Tassone, D. M. Delongchamp, G. G. Malliaras, *Nat. Commun.* **2016**, *7*, 11287.
[37] E. Stavrinidou, P. Leleux, H. Rajaona, D. Khodagholy, J. Rivnay, M. Lindau, S. Sanaur, G. G. Malliaras, *Adv. Mater.* **2013**, *25*, 4488.
[38] S. Zhang, E. Hubis, C. Girard, P. Kumar, J. DeFranco, F. Cicoira, *J. Mater. Chem. C* **2016**, *4*, 1382.
[39] E. W. Paul, A. J. Ricco, M. S. Wrighton, *J. Phys. Chem.* **1985**, *89*, 1441.
[40] H. S. White, G. P. Kittlesen, M. S. Wrighton, *J. Am. Chem. Soc.* **1984**, *106*, 5375.
[41] N. D. Robinson, P.-O. Svensson, D. Nilsson, M. Berggren, *J. Electrochem. Soc.* **2006**, *153*, H39.
[42] D. A. Bernards, G. G. Malliaras, *Adv. Funct. Mater.* **2007**, *17*, 3538.
[43] D. Tu, L. Kergoat, X. Crispin, M. Berggren, R. Forchheimer, *Proc. SPIE* **2012**, *8478*, 84780L, DOI: 10.1117/12.929886.
[44] D. Tu, L. Herlogsson, L. Kergoat, X. Crispin, M. Berggren, R. Forchheimer, *IEEE Trans. Electron Devices* **2011**, *58*, 3574.
[45] M. R. Abidian, D. C. Martin, *Biomaterials* **2008**, *29*, 1273.
[46] S. Venkatraman, J. Hendricks, Z. A. King, A. J. Sereno, S. Richardson-Burns, D. Martin, J. M. Carmena, *IEEE Trans. Neural Syst. Rehabil. Eng.* **2011**, *19*, 307.
[47] Y. Tsividis, J. Milios, *J. Electroanal. Chem.* **2013**, *707*, 156.
[48] J. Bobacka, A. Lewenstam, A. Ivaska, *J. Electroanal. Chem.* **2000**, *489*, 17.
[49] E. Stavrinidou, P. Leleux, H. Rajaona, M. Fiocchi, S. Sanaur, G. G. Malliaras, *J. Appl. Phys.* **2013**, *113*, 244501.
[50] D. Braga, N. C. Erickson, M. J. Renn, R. J. Holmes, C. D. Frisbie, *Adv. Funct. Mater.* **2012**, *22*, 1623.
[51] J. Rivnay, P. Leleux, M. Sessolo, D. Khodagholy, T. Herve, M. Fiocchi, G. G. Malliaras, *Adv. Mater.* **2013**, *25*, 7010.
[52] J. T. Friedlein, S. E. Shaheen, G. G. Malliaras, R. R. McLeod, *Adv. Electron. Mater.* **2015**, *1*, 1500189.
[53] Q. Wei, M. Mukaida, K. Kirihara, Y. Naitoh, T. Ishida, *ACS Appl. Mater. Interfaces* **2016**, *8*, 2054.
[54] P. Barthó, H. Hirase, L. Monconduit, M. Zugaro, K. D. Harris, G. Buzsáki, *J. Neurophysiol.* **2004**, *92*, 600.
[55] S. Inal, J. Rivnay, P. Leleux, M. Ferro, M. Ramuz, J. C. Brendel, M. M. Schmidt, M. Thelakkat, G. G. Malliaras, *Adv. Mater.* **2014**, *26*, 7450.
[56] E. Zeglio, M. Vagin, C. Musumeci, F. N. Ajjan, R. Gabrielsson, X. T. Trinh, N. T. Son, A. Maziz, N. Solin, O. Inganäs, *Chem. Mater.* **2015**, *27*, 6385.
[57] B. D. Paulsen, C. D. Frisbie, *J. Phys. Chem. C* **2012**, *116*, 3132.
[58] D. Khodagholy, J. N. Gelinas, T. Thesen, W. Doyle, O. Devinsky, G. G. Malliaras, G. Buzsaki, *Nat. Neurosci.* **2015**, *18*, 310.
[59] C. Gold, D. A. Henze, C. Koch, G. Buzsáki, *J. Neurophysiol.* **2006**, *95*, 3113.
[60] B. Winther-Jensen, B. Kolodziejczyk, O. Winther-Jensen, *APL Mater.* **2015**, *3*, 014903.
[61] X. Wang, B. Shapiro, E. Smela, *J. Phys. Chem. C* **2009**, *113*, 382.
[62] X. Wang, E. Smela, *J. Phys. Chem. C* **2009**, *113*, 369.
[63] G. Greczynski, T. Kugler, M. Keil, W. Osikowicz, M. Fahlman, W. R. Salaneck, *J. Electron Spectrosc. Relat. Phenom.* **2001**, *121*, 1.
[64] S. Möller, S. R. Forrest, C. Perlov, W. Jackson, C. Taussig, *J. Appl. Phys.* **2003**, *94*, 7811.
[65] P. Kumar, Z. Yi, S. Zhang, A. Sekar, F. Soavi, F. Cicoira, *Appl. Phys. Lett.* **2015**, *107*, 053303.
[66] J. Lee, *Appl. Phys. Lett.* **2016**, *108*, 203302.
[67] F. Gentile, D. Delmonte, M. Solzi, M. Villani, S. Iannotta, A. Zappettini, N. Coppedè, *Org. Electron.* **2016**, *35*, 59.
[68] J. A. DeFranco, B. S. Schmidt, M. Lipson, G. G. Malliaras, *Org. Electron.* **2006**, *7*, 22.